BIOCHEMISTRY
including biophysical chemistry & molecular biology
Article

Biochemistry **2009,** *48,* 11737–11744 11737
DOI: 10.1021/bi901349z

Pre-Steady-State Kinetic Analysis of *cis*-3-Chloroacrylic Acid Dehalogenase: Analysis and Implications†

Brooklyn A. Robertson,‡ Gottfried K. Schroeder,§ Zhinan Jin,‡,∥ Kenneth A. Johnson,*,‡,∥ and Christian P. Whitman*,§,∥

‡*Department of Chemistry and Biochemistry and* ∥*Institute for Cellular and Molecular Biology and* §*Division of Medicinal Chemistry, College of Pharmacy, University of Texas, Austin, Texas 78712*

Received August 4, 2009; Revised Manuscript Received October 23, 2009

ABSTRACT: Isomer-specific 3-chloroacrylic acid dehalogenases catalyze the hydrolytic dehalogenation of the *cis*- and *trans*-isomers of 3-chloroacrylate to yield malonate semialdehyde. These reactions represent key steps in the degradation of the nematocide, 1,3-dichloropropene. The kinetic mechanism of *cis*-3-chloroacrylic acid dehalogenase (*cis*-CaaD) has now been examined using stopped-flow and chemical-quench techniques. Stopped-flow analysis of the reaction, following the fluorescence of an active site tryptophan, is consistent with a minimal three-step model involving substrate binding, chemistry, and product release. Chemical-quench experiments show burst kinetics, indicating that product release is at least partially rate limiting. Global fitting of all of the kinetic results by simulation is best accommodated by a four-step mechanism. In the final kinetic model, the enzyme binds substrate with an immediate isomerization to an alternate fluorescent form and chemistry occurs, followed by the ordered release of two products, with the release of the first product as the rate-limiting step. Bromide ion is a competitive inhibitor of the reaction indicating that it binds to the free enzyme rather than to the enzyme with one product still bound. This observation suggests that malonate semialdehyde is the first product released by the enzyme (rate limiting), followed by halide. A comparison of the unliganded *cis*-CaaD crystal structure with that of an inactivated *cis*-CaaD where the prolyl nitrogen of Pro-1 is covalently attached to (*R*)-2-hydroxypropanoate provides a possible explanation for the isomerization step. The structure of the covalently modified enzyme shows that a seven-residue loop comprised of residues 32−38 is closed down on the active site cavity where the backbone amides of two residues (Phe-37 and Leu-38) interact with the carboxylate group of the adduct. In the unliganded form, the same loop points away from the active site cavity. Similarly, substrate binding may cause this loop to close down on the active site and sequester the reaction from the external environment.

The catabolism of 1,3-dichloropropene (**1**, Scheme 1) in *Pseudomonas pavonaceae* 170 and coryneform bacterium strain FG41 involves the hydrolytic dehalogenation of *cis*- and *trans*-3-chloroacrylate (**2** and **3**, respectively) resulting in malonate semialdehyde (**4**) (*1*−*3*). An enzyme-catalyzed decarboxylation of the β-keto acid yields acetaldehyde (**5**), which is likely routed to the Krebs cycle (*3*). Each isomer of 3-chloroacrylate is converted to **4** by a separate dehalogenase known as *cis*- or *trans*-3-chloroacrylic acid dehalogenase (*cis*-CaaD[1] and CaaD, respectively) (*4*, *5*). The two enzymes belong to different families in the tautomerase superfamily and share a common β-α-β building block and a catalytic amino-terminal proline (*6*, *7*).

In the current working hypotheses for the *cis*-CaaD and CaaD mechanisms, four common active site residues play key catalytic roles (Scheme 2). In CaaD, a heterohexamer made up of three α-subunits and three β-subunits, αGlu-52 abstracts hydrogen from water for addition to C-3 of **3**, and a pair of arginines (αArg-8 and αArg-11) interacts with the C-1 carboxylate group (*4*, *5*, *8*−*11*). This interaction binds and polarizes the substrate to facilitate the attack of water at C-3. The addition of water to the double bond of **3** is completed with the delivery of a proton to C-2 by βPro-1, functioning as a general acid catalyst. A similar sequence of events is proposed for the trimeric *cis*-CaaD where the corresponding residues are Pro-1, Arg-70, Arg-73, and Glu-114 (*5*, *11*).

In the proposed catalytic mechanism, the polarization of **3** and addition of water generate an enediolate species (**6**, Scheme 2). Subsequent tautomerization and protonation at C-2 (route A) result in an unstable chlorohydrin intermediate (**7**), which can undergo chemical or enzymatic decay to afford **4** and HCl. Alternatively, the enediolate species can expel the chloride ion (i.e., an α,β-elimination), as shown in route B, to form the enol intermediate, **8**. Tautomerization of **8** produces **4**. Experiments showing that the ketonization of phenylenolpyruvate to phenylpyruvate is kinetically competent in the overall CaaD reaction are consistent with route B, but not conclusive (*12*).

†This research was supported by National Institutes of Health Grant GM-65324 and the Robert A. Welch Foundation (F-1334 and F-1604). The Analytical Instrumentation Facility Core (College of Pharmacy, The University of Texas at Austin) is supported by NIH Center Grant ES07784.

*Corresponding authors. K.A.J.: tel, (512) 471-0434; fax, (512) 471-0435; e-mail, kajohnson@mail.utexas.edu. C.P.W.: tel, (512) 471-6198; fax, (512) 232-2606; e-mail, whitman@mail.utexas.edu.

[1]Abbreviations: CaaD and *cis*-CaaD, *trans*- and *cis*-3-chloroacrylic acid dehalogenase, respectively; DhlA, haloalkane dehalogenase from *Xanthobacter autotrophicus*; ESI-MS, electrospray ionization mass spectrometry; IC, ion chromatography; ppb, parts per billion; ppm, parts per million; SDS−PAGE, sodium dodecyl sulfate−polyacrylamide gel electrophoresis.

Published on Web 10/26/2009

Scheme 1

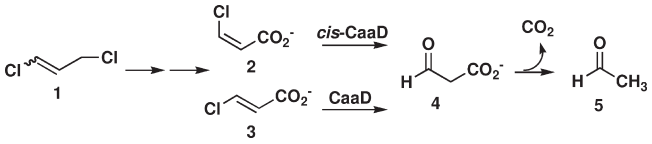

In addition to the different quaternary structures (i.e., heterohexamer vs trimer), there are mechanistic distinctions between CaaD and *cis*-CaaD. Crystallographic studies of *cis*-CaaD identified His-28 and Tyr-103 as two additional residues that assist catalysis (*11*). The positions of these residues in the structures suggested that Tyr-103 and Glu-114 activate water, and His-28, along with the arginine pair, binds and polarizes the substrate. Mutagenesis analysis also suggests that the residues involved in water activation might be more critical for CaaD catalysis, whereas the residues responsible for substrate activation play a more significant role in the *cis*-CaaD mechanism. For example, replacing αGlu-52 of CaaD with a glutamine renders the enzyme totally inactive, but the analogous mutation in *cis*-CaaD only diminishes activity. Likewise, replacing Arg-70 or Arg-73 with an alanine completely eliminates *cis*-CaaD activity, but the corresponding mutations in CaaD do not. Pro-1 is critical for both activities.

Mutant analysis has provided a measure of the relative importance of the key catalytic residues, but it has not generally been informative because most mutants show little or no measurable activity in steady-state kinetic assays. For these reasons and the fact that many details of catalysis are not well understood, a pre-steady-state kinetic analysis of both the enzyme wild-type- and mutant-catalyzed reactions is being pursued. The analysis for wild-type *cis*-CaaD has now been completed using the kinetically equivalent substrate, *cis*-3-bromoacrylic acid (**9**). This ligand was used in place of **2** because bromide (rather than chloride, a very common contaminant) is more readily quantified in chemical-quench experiments. The stopped-flow enzyme fluorescence data fit to a double exponential equation, which is consistent with a minimum of two kinetically significant steps preceding product release in the overall mechanism (net three steps). Ion chromatography (IC) methodology to quantify bromide ion release in the reaction was developed and used in the analysis of chemical-quench mixtures. A burst of bromide ion release followed by steady-state turnover was observed. These observations are consistent with the rate-limiting release of product. Global fitting of the combined data directly by simulation avoids the underlying assumptions and simplification required for conventional analysis and provides a minimal four-step model with the individual rate constants for chemistry and ordered product release. These results set the stage for the analysis of CaaD and the mutants of both dehalogenases.

EXPERIMENTAL PROCEDURES

Materials. Chemicals, biochemicals, buffers, and solvents were purchased from Sigma-Aldrich Chemical Co. (St. Louis, MO), Fisher Scientific Inc. (Pittsburgh, PA), Fluka Chemical Corp. (Milwaukee, WI), or EMD Chemicals, Inc. (Gibbstown, NJ). Reagents used for the ion chromatography (IC) and rapid-quench experiments were at least 99.99% pure or greater, as indicated by the manufacturer. The PolyVial vials (0.5 mL), filter caps, and automated sampler cassettes (0.5 mL) were purchased from Dionex Corp. (Sunnyvale, CA). The Microcon centrifugal filter devices (3000 MW cutoff), the Amicon stirred cells, and the YM3 and YM10 ultrafiltration membranes were purchased from Millipore Corp. (Billerica, MA). Prepacked PD-10 Sephadex G-25 columns were purchased from Biosciences AB (Uppsala, Sweden). The construction of the *cis*-CaaD expression plasmid is described elsewhere (*5*).

General Methods. Mass spectral data were obtained on an LCQ electrospray ion-trap mass spectrometer (Thermo, San Jose, CA) in the Analytical Instrumentation Facility Core in the College of Pharmacy at the University of Texas at Austin. Steady-state kinetic parameters were obtained at 22 °C on an Agilent 8453 diode-array spectrophotometer. Nonlinear regression data analysis was performed using the program Grafit (Erithacus Software Ltd., Staines, U.K.) obtained from Sigma-Aldrich. The pre-steady-state kinetic data were fit by simulation using KinTek Global Kinetic Explorer (Kintek Corp., Austin, TX) (*13*, *14*). Protein concentrations were determined by the method of Waddell (*15*). Proteins were analyzed by sodium dodecyl sulfate−polyacrylamide gel electrophoresis (SDS−PAGE) under denaturing conditions on gels containing 15% polyacrylamide (*16*).

Purification and Characterization of cis-CaaD. *cis*-CaaD was produced in *Escherichia coli* BL21-Gold(DE3) cells and purified to homogeneity (as assessed by SDS−PAGE) by published protocols (*5*). Typically, this protocol yielded ∼100 mg of purified enzyme from ∼5 g of cells. Electrospray ionization mass spectrometry (ESI-MS) analysis of the protein showed a mass of 16622 Da (calculated 16624 Da), indicating that the initiating *N*-formylmethionine had been posttranslationally removed from the protein. The enzyme was stored in 10 mM Tris−SO_4 buffer (pH 9.0) and exchanged into the indicated buffers before use.

Steady-State Kinetics. The steady-state kinetic parameters for *cis*-CaaD were measured for **2** and *cis*-3-bromoacrylic acid (**9**) using a previously described assay (*5*), modified as follows. The assays were carried out at 22 °C in 20 mM Na_2HPO_4 buffer or 20 mM $NaHCO_3$ buffer, pH 9.0. A 25 mL solution of enzyme (2 μM based on monomer mass) was made up in each buffer and allowed to equilibrate at 22 °C for 1 h. The assay was initiated by the addition of substrate (**2** or **9**, 10−700 μM), obtained from a 10 or 50 mM stock solution made up in 100 mM Na_2HPO_4 buffer, pH 9.0, or 50 mM $NaHCO_3$ buffer, pH 10. Typically, the addition of substrate (as the free acid) to the 100 mM Na_2HPO_4 buffer adjusted the pH of the stock solution from 9.0 to 7.3 and the pH of the 50 mM $NaHCO_3$ buffer from 10 to 7.5. The 10 mM stock solutions were made by diluting an aliquot of the 50 mM stock solutions into 100 mM NaH_2PO_4 buffer, pH 7.3. The decrease in absorbance at 224 nm, corresponding to the hydration of **2** ($\varepsilon = 2900\ M^{-1}\ cm^{-1}$) or **9** ($\varepsilon = 3600\ M^{-1}\ cm^{-1}$) (*5*), was monitored over a 40 s time period, recording readings every 1.5 s. Initial rates (measured from the first 16 s) were plotted vs substrate concentration and fit to the Michaelis−Menten equation using Grafit to determine the values of k_{cat} and K_m.

Ion Chromatography. The dehalogenation of *cis*-3-bromoacrylate in the chemical-quench experiments was quantified by measuring the bromide ion concentration with ion chromatography (IC). This analysis was carried out on a Dionex ion chromatography system (ICS-1500; Dionex Corp.) equipped with an AG12A precolumn (4 × 40 mm), an IonPac AS12A column (4 × 200 mm), an anion self-regenerating suppressor (ASRS ULTRA II, 4 mm), and an AS40 autosampler. Anion detection was performed by electrical conductivity. A solution of 2.7 mM Na_2CO_3/0.3 mM $NaHCO_3$ (pH 9.6) was used as the eluent at a flow rate of 1.5 mL/min.

Scheme 2

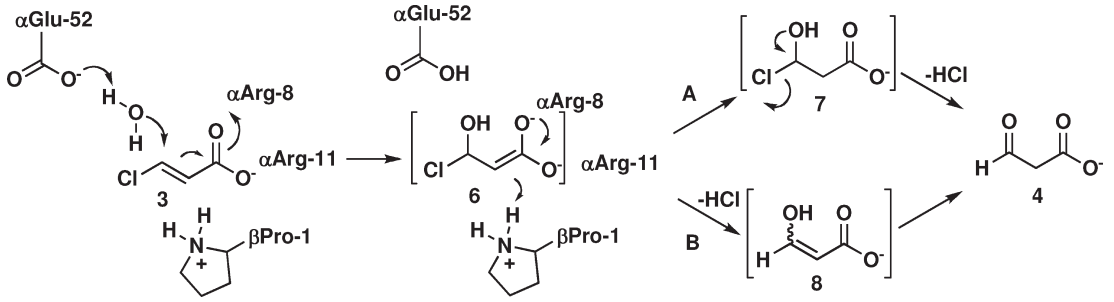

Calibration Curve for Ion Chromatography. The calibration curve for the bromide ion analysis was constructed using eight known concentrations of bromide ion (0−10 ppm) made from a standard solution of NaBr (Fluka bromide IC standard solution, 1 g/L, 1000 ppm bromide ion) in 20 mM $NaHCO_3$ buffer, pH 9.0. A 10 ppm solution of bromide ion (2 mL) was made from the stock solution by diluting 20 μL into 1980 μL of 20 mM $NaHCO_3$ buffer, pH 9.0. This solution was then used to make seven serial dilutions (2 mL each) with the following bromide ion concentrations: 5, 2.5, 1.25, 0.625, 0.3125, 0.0156, and 0 ppm (i.e., 20 mM $NaHCO_3$ buffer, pH 9.0).

Stopped-Flow Experiments. The stopped-flow experiments were carried out on a SF 2004 series stopped-flow apparatus donated by Kintek Corp. The enzyme *cis*-CaaD (20 μM based on monomer molecular mass) was made up in 20 mM $NaHCO_3$ buffer, pH 9.0, and allowed to equilibrate at 22 °C for 1 h. Various concentrations of **9** (25−50000 μM) were made up in 50 mM $NaHCO_3$ buffer, pH 10.0. The enzyme (10 μM after mixing) and substrate (12.5−25000 μM after mixing) solutions were then mixed in the stopped-flow apparatus at 22 °C. The pH after mixing was 7.8, at the highest substrate concentration. The fluorescence was excited at 280 nm, and a 340 nm long pass filter was used to observe emission. The slit width on both the monochromator and the light filter was set at 3.16 mm. Time courses were the average of five runs at each substrate concentration. The time courses were 1 or 2 s in duration, with 1000 data points collected for each trace. To determine whether the fluorescence signal returned to its initial fluorescence value, the reaction was monitored for longer time periods (ranging from 12 to 180 s in duration) at selected substrate concentrations. However, these data were not used in the global fitting. Stopped-flow fluorescence time courses were fit initially with the nonlinear regression program Grafit using the kinetic schemes and equations found in the Supporting Information and then subsequently fit globally using the KinTek Explorer software.

Rapid-Quench Experiments. The rapid-quench experiments were carried out at 22 °C on a quench-flow apparatus (RFQ-3) donated by Kintek Corp. Typically, one syringe was loaded with *cis*-CaaD (250, 500, or 1000 μM made up in 20 mM $NaHCO_3$ buffer, pH 9.0), and another syringe was loaded with freshly prepared *cis*-3-bromoacrylic acid (10000 μM made up in 50 mM $NaHCO_3$ buffer, pH 10.0). Each reaction was initiated by the rapid mixing of aliquots (15 μL) of the reactants from both syringes. The reaction mixture was quenched at various intervals ranging from 3 to 750 ms with an equal volume of 0.6 M H_2SO_4. The individually quenched reaction mixtures were centrifuged at 1000 rpm for 5 s, and the supernatant was transferred to a 1.5 mL Eppendorf tube equipped with a Microcon centrifugal filter device (3000 MW cutoff). The samples were centrifuged at 9000 rpm for 50 min to remove the enzyme from the reaction mixtures. A 20 μL aliquot of the flow-through was diluted into 780 μL of 20 mM $NaHCO_3$ buffer, pH 9.0, to give a final volume of 800 μL. A 400 μL portion of each quenched mixture was loaded into 500 μL sample vials (Dionex) and placed in an AS40 autosampler. An aliquot (10 μL) of sample from each vial was loaded onto the AS12A column by the autosampler. The column had been previously equilibrated with 2.7 mM Na_2CO_3/0.3 mM $NaHCO_3$ buffer, pH 9.6. The contents of the mixture were eluted isocratically (1.5 mL/min) over a 15 min period. The bromide ion was detected by suppressed conductivity using an electrochemical detector with an applied current of 100 mA. The samples were alternated with deionized water samples (400 μL) in order to elute any remaining anions from the column before loading the next sample.

The data were fit to the burst equation (eq 1)

$$[P]_{obs} = Ae^{-\lambda t} + k_{ss}t + C \quad (1)$$

where $[P]_{obs}$ is the observed concentration of product bromide, A is the burst amplitude (A_0) times the active enzyme concentration ($[E]_0$), λ is the burst rate constant, k_{ss} is the steady-state turnover rate (approaching k_{cat} at saturating substrate) times the active enzyme concentration ($[E]_0$), and C is a constant (*17*).

Reversible Inhibition of cis-CaaD by Bromide Ion. *cis*-CaaD (17 mg/mL) was diluted into 75 mL of 20 mM $NaHCO_3$ buffer, pH 9.0, to give a final enzyme concentration of ~2 μM (in monomer). Subsequently, an aliquot of inhibitor from a stock solution (0.5 M in 20 mM $NaHCO_3$ buffer, pH 9.0) was added to the diluted enzyme solution to yield a total of eight final inhibitor concentrations (0, 0.05, 0.1, 0.5, 2, 5, 15, and 30 mM). After 1 h, aliquots (1 mL) of each solution were removed and assayed using **9** (50−500 μM). Steady-state parameters were determined as described above. The mode of inhibition was determined from the patterns observed in the Dixon plot ($1/v$ as a function of inhibitor concentration at various substrate concentrations) and the plot of S/v versus inhibitor concentration at various substrate concentrations (*18*−*20*). The inhibition constant (K_i) was determined from the intersection point in the Dixon plot.

Data and Global Fitting Analysis. Conventional data fitting of pre-steady-state kinetic data (including the concentration dependence) by nonlinear regression using the program Grafit provided initial estimates for rate constants and a minimal number of steps in the overall reaction pathway. The steady-state k_{cat}/K_m value was used as a lower limit for the rate of substrate binding, and the k_{cat} value furnished a lower limit for any individual first-order rate constants following substrate binding and proceeding through product release (*17*). The pre-steady-state data from both sets of experiments were then fit to a single kinetic model by an iterative, trial and error global fitting process

Table 1: Steady-State Kinetic Parameters for *cis*-CaaD in Na_2HPO_4 and $NaHCO_3$ Buffers[a]

enzyme	substrate	buffer	K_m (μM)	k_{cat} (s^{-1})	k_{cat}/K_m (M^{-1} s^{-1})
cis-CaaD	**2**	20 mM Na_2HPO_4	200 ± 15	5.9 ± 0.1	2.9×10^4
cis-CaaD	**9**	20 mM Na_2HPO_4	200 ± 17	5.4 ± 0.2	2.7×10^4
cis-CaaD	**9**	20 mM $NaHCO_3$	300 ± 32	2.4 ± 0.1	8.1×10^3

[a]Assay conditions are provided in the text. Errors are standard deviations.

using the computer program KinTek Global Kinetic Explorer, which utilizes direct numerical integration to simulate experimental results (*13*). This feature of the program coupled with the error analysis functionality of FitSpace (*14*), also a component of KinTek Explorer, was utilized to evaluate the goodness of fit and the degree to which the individual rate constants were constrained by the data. The Supporting Information details the process of deriving the final best fit by global analysis and shows how we reconcile some unusual features of the data observed in conventional fitting.

RESULTS

Steady-State Kinetic Parameters for cis-CaaD. The steady-state kinetic parameters for *cis*-CaaD using *cis*-3-chloro- and *cis*-3-bromoacrylate (**2** and **9**, respectively) were measured in 20 mM Na_2HPO_4 buffer and in 20 mM $NaHCO_3$ buffer, pH 9.0. The K_m and k_{cat} values for **2** and **9** were comparable in the Na_2HPO_4 buffer but different from those measured in the $NaHCO_3$ buffer (Table 1). In 20 mM $NaHCO_3$ buffer, there is a 1.5-fold increase in K_m and a 2.2-fold decrease in k_{cat}. This resulted in a 3.3-fold decrease in the value of k_{cat}/K_m. The basis for this difference is not known, but it can be reasonably ascribed to modest bicarbonate inhibition via the carboxylate group. Although the dehalogenase reaction is more efficient (as assessed by the k_{cat}/K_m values) in the phosphate buffer, it was observed in the course of IC methodology development (for the chemical-quench experiments) that the signals for phosphate and bromide ion overlap (data not shown). Hence, bicarbonate buffer was subsequently used for the chemical-quench experiments. For consistency, the stopped-flow experiments were also carried out in the same bicarbonate buffer.

Quantification of Bromide Ion Concentration by Ion Chromatography. The bromide ion concentration in the burst experiments was quantified by ion chromatography. The components of a typical burst experiment (*cis*-3-bromoacrylate, bromide, and sulfate from the H_2SO_4 quench) are clearly separated and elute in the order indicated using 2.7 mM Na_2CO_3/0.3 mM $NaHCO_3$, pH 9.6, as the eluent at a flow rate of 1.5 mL/min (Figure 1). The sulfate peak (data not shown) typically elutes after ~11 min. The detection limits for bromide ion ranged from 7.5 ppb (92 nM) to 25 ppm (313 μM).

Stopped-Flow Experiments. Stopped-flow fluorescence experiments were carried out to determine the kinetics of *cis*-3-bromoacrylic acid (**9**) binding to *cis*-CaaD and subsequent turnover in 20 mM $NaHCO_3$ buffer. There are two tryptophan residues in *cis*-CaaD, and crystal structures show that one tryptophan is on the protein surface (Trp-128) whereas the other tryptophan resides within the active site cavity (Trp-101) (*11*). As such, Trp-101 is poised to report on changes in the active site cavity. Accordingly, the tryptophan fluorescence emission signal

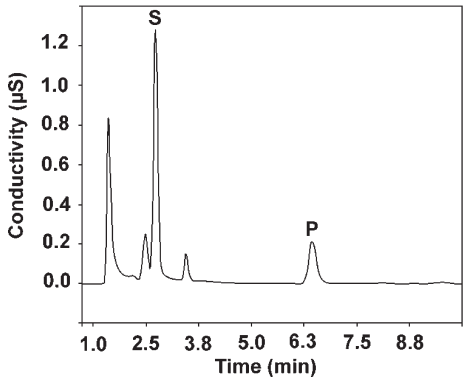

FIGURE 1: Representative ion chromatograph of a quenched reaction mixture from a rapid-quench experiment using *cis*-CaaD and **9** in 20 mM $NaHCO_3$ buffer, pH 9.0. The labeled peaks S and P correspond to **9** and bromide ion, respectively. The unlabeled peaks are unidentified buffer components. The eluting conditions are described in the text.

was monitored during the course of substrate binding, catalysis, and product release. In these experiments, *cis*-CaaD (10 μM) and various concentrations of **9** (12.5−25000 μM where the reported concentrations are those after mixing) were rapidly mixed in a stopped-flow instrument in 20 mM $NaHCO_3$ buffer, pH 9.0.[2]

At all substrate concentrations, the traces (1−2 s) show a fast initial fluorescence decrease followed by a slow decrease (Figure 2A) and fit satisfactorily to a double exponential equation (eq S1). The substrate concentration dependence of λ_1, the rate constant for the fast phase (Figure S1A), is linear and has a nonzero intercept (eq S2). This linear relationship is indicative of at least one step, and the nonzero intercept implies that the step is reversible (*17*). The dependence of the rate constant for the slow phase, λ_2, on substrate concentration is hyperbolic (eq S3), following a brief initial sigmoidal concentration dependence at the lowest concentrations of substrate (Figure S1B). The hyperbolic substrate concentration dependence of the slow phase (ignoring the initial sigmoidal portion as discussed in sections S2 and S3 in the Supporting Information), taken together with the nonzero intercept, is consistent with a reversible two-step minimal mechanism (Scheme S1) (*17*). The substrate dependence of the amplitude of both phases is plotted in Figure S1C,D. Both are concentration dependent, but the fast phase dominates the overall amplitude signal at high substrate concentrations. Although a single exponential is generally expected for each individual step in the overall mechanism, in the presence of excess substrate, product release to regenerate free enzyme will not contribute a new exponential phase (*17*). Therefore, the stopped-flow fluorescence data alone are consistent with the minimal three-step reaction pathway shown in Scheme 3. Additionally, subsequent steps with similar rates (within a factor of 4), or two steps involving an initial weak binding step followed by a rapid isomerization, can collapse to a single exponential which may be difficult to resolve by conventional analysis (*13*). A more complete treatment of the conventional analysis can be found in the Supporting Information.

[2]Experiments conducted for longer time periods (12−180 s) suggested that the fluorescence did not return to its initial value, consistent with product inhibition. However, it was not possible to assess this accurately (and the data at these longer time periods were not included in the fit) because the reactions at high substrate concentrations did not go to completion within these time periods.

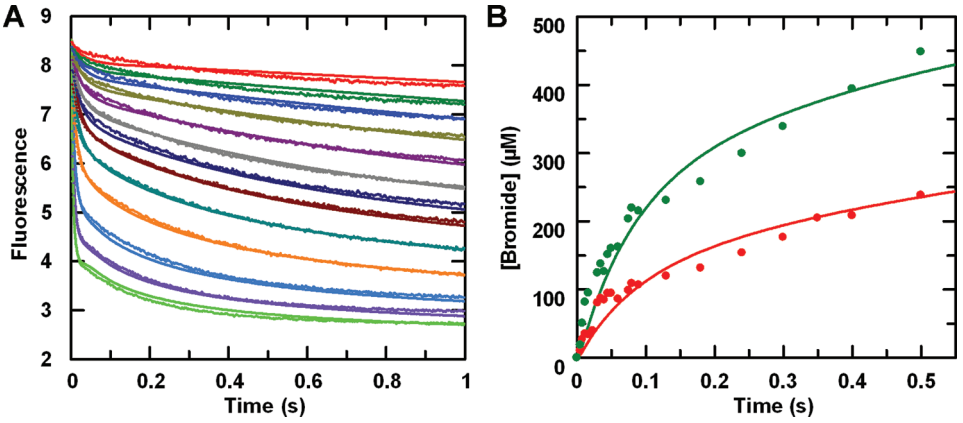

FIGURE 2: The *cis*-CaaD transient kinetic data fit globally to the single mechanism shown in Scheme 4 (solid line). (A) Stopped-flow fluorescence traces at various substrate concentrations (125−10500 μM). For clarity, not all of the traces are shown. (B) Rapid-quench results for two concentrations of *cis*-CaaD (125 and 250 μM)[3] and a saturating substrate concentration. In both panels, the smooth lines were computed by numerical integration based upon the best global fit using Scheme 4 and the rate constants in Table 3.

Scheme 3

$$E + S \underset{k_{-1}}{\overset{k_1}{\rightleftharpoons}} ES \underset{k_{-2}}{\overset{k_2}{\rightleftharpoons}} EPQ \underset{k_{-3}}{\overset{k_3}{\rightleftharpoons}} E + P + Q$$

Chemical-Quench Experiments of the cis-CaaD-Catalyzed Reaction. In order to identify the rate-limiting step, pre-steady-state burst experiments were conducted on the *cis*-CaaD reaction. Three experiments were initiated by mixing different concentrations of *cis*-CaaD (final concentrations 125, 250, and 500 μM) with an excess of *cis*-3-bromoacrylic acid (final concentration 5 mM). At fixed time intervals (3−750 ms), the reactions were quenched, and the amount of bromide ion was quantified.

A pre-steady-state burst of product (i.e., bromide ion) was observed in all three experiments when the concentration of bromide ion was plotted versus time (Figure 2B), with a fast initial rate followed by a slower steady-state rate of product formation. The presence of a burst indicates that some step other than chemistry is at least partially rate limiting (presumably product release). If chemistry were rate limiting, then no burst would be seen and the amount of product would increase linearly at a steady-state rate (k_{ss}) (*17*). Fitting the rapid-quench data to the general burst equation (eq 1) yielded burst rate constants (λ) of 41.4 ± 7.8, 36.2 ± 4.5, and 24.4 ± 1.8 s^{-1} for the experiments using 125, 250, and 500 μM enzyme, respectively. On the basis of a *minimal model*, the burst rate constant (λ) should represent a sum of all the forward and reverse rates for all of the chemical steps after substrate binding (for instance, loop movement and chemistry) in addition to the rates of product release (section S1, Supporting Information). The steady-state turnover rates (k_{cat}), calculated from the parameters determined in these experiments, are 3.8, 3.6, and 5.0 s^{-1}, respectively. The k_{cat} values were obtained by dividing k_{ss} by the active enzyme concentrations, obtained from the amplitude of the burst. These values are generally in good agreement with the steady-state k_{cat} values reported above for *cis*-CaaD and *cis*-3-bromoacrylate (in 20 mM $NaHCO_3$ buffer at pH 9.0).[3] The other fitted parameters from eq 1 are summarized in Table 2.

Table 2: Parameters Obtained from Burst Experiments

[*cis*-CaaD] (μM)	burst rate k_1 (s^{-1})	steady-state rate k_2 (μM s^{-1})	burst amplitude A (μM)	k_{cat} (s^{-1}) calcd from burst expt
125	41.4 ± 7.8[a]	316 ± 21	82 ± 6	3.8 ± 0.1
250	36.2 ± 4.5	577 ± 29	162 ± 8	3.6 ± 0.07
500	24.4 ± 1.8	1789 ± 48	359 ± 16	5.0 ± 0.05

[a]Errors are standard deviations.

Reversible Inhibition of cis-CaaD by Bromide Ion. In order to determine the order of product release (malonate semialdehyde vs bromide), the inhibition of *cis*-CaaD by bromide was examined. Two plots were generated (Figure S2). The plot of S/v versus inhibitor concentration displays parallel lines, and the Dixon plot shows intersecting lines. Taken together, these observations are indicative of competitive inhibition (i.e., a direct interaction with the free enzyme) and suggest that halide is the second product to come off the enzyme ($K_i \sim 20$ mM) (*18*−*20*). Steady-state time courses at a fixed concentration of substrate (200 μM) and increasing concentrations of bromide were also used in global fitting (data not shown) to fit the rate of product rebinding (i.e., k_{-4} in Scheme 4).

Global Fitting Analysis. A three-step mechanism such as the one shown in Scheme 3 was used to fit the data initially, but it could not account for all of the experimental results, so an additional step was required. In particular, as described in detail in the Supporting Information, the concentration dependence of the amplitude and the unusual sigmoid concentration dependence of the rate of the slow phase of the fluorescence transient were inconsistent with Scheme 3. In order to generate an accurate fit to the stopped-flow data, it was necessary to include an additional step as shown in Scheme 4, where the enzyme form, F, had a 4-fold lower fluorescence intensity relative to the original form of the enzyme, E. It also proved necessary to adjust the model for the release of product in two separate steps and to account for product inhibition even during the transient kinetic

[3]The calculated steady-state rate k_{cat} (5 s^{-1}) at the highest enzyme concentration (500 μM) is somewhat faster than that seen at lower enzyme concentrations (3.8 and 3.6 s^{-1}). The faster rate could be a result of a drop in pH due to the release of HBr, which may accelerate the reaction. Previous work has shown that the optimal pH for the *cis*-CaaD-catalyzed reaction is at pH ~8 (*21*). It is possible that the higher quantity of HBr generated at the higher enzyme concentration exceeded the buffering capacity of bicarbonate buffer. Therefore, a drop in pH could lead to a faster than anticipated steady-state rate, compared with the other data collected at pH 9.0. For these reasons, the rapid-quench results obtained at 500 μM were not used in the global fit.

Table 3: Kinetic Rate Constants for the *cis*-CaaD Reaction Derived from the Global Analysis Fit[a]

rate	lower limit	upper limit	average[b]	rate	lower limit	upper limit	average
k_1	–[c]	–[c]	$0.025 \pm 0.005\ \mu M^{-1}\ s^{-1}$	k_{-1}	142	212	$177 \pm 35\ s^{-1}$
k_2	30	60	$45 \pm 15\ s^{-1}$	k_{-2}	–[d]	–[d]	–[d]
k_3	12.1	22	$17 \pm 5\ s^{-1}$	k_{-3}	6.3	10.6	$8.5 \pm 2.2\ \mu M^{-1}\ s^{-1}$
k_4	64	105	$85 \pm 21\ s^{-1}$	k_{-4}	n/a	n/a	$5 \times 10^{-4}\ \mu M^{-1}\ s^{-1}$

[a]The data are fit globally to the mechanism shown in Scheme 4, as described in the text. [b]The errors are standard deviations. FitSpace error confidence contours can be found in the Supporting Information (Figure S3). [c]The value of k_1 was determined as described in the Supporting Information. [d]For the model in Scheme 4, the chemistry step is assumed to be largely irreversible. Therefore, the value for the rate constant k_{-2} was fixed at zero in the global fitting process. Additional fitting trials did yield values for k_{-2} ($0.5-5\ s^{-1}$). However, the values were not well constrained, indicating that the data are not sufficient to accurately resolve this parameter.

Scheme 4

$$E + S \underset{k_{-1}}{\overset{k_1}{\rightleftharpoons}} FS \underset{k_{-2}}{\overset{k_2}{\rightleftharpoons}} FPQ \underset{k_{-3}}{\overset{k_3}{\rightleftharpoons}} EQ + P;\ EQ \underset{k_{-4}}{\overset{k_4}{\rightleftharpoons}} E + Q$$

experiments. Ultimately, a minimal model with four kinetically distinguishable steps was required to fit all of the data (Scheme 4), where E is enzyme, F is the second fluorescent form of the enzyme, S is substrate, and Q and P are the two products of the reaction. (See the Supporting Information for additional details on the fitting process.)

The model implies that after binding substrate the intrinsic fluorescence of the enzyme changes (to F), chemistry occurs, the first product is released, and the enzyme relaxes back to the resting fluorescent state (E), prior to the release of the second product, but this is not known with certainty.[4] The global fit parameters, along with error estimates, calculated using FitSpace (*14*), are summarized in Table 3.[5] FitSpace error confidence contours and a treatment of the results can be found in the Supporting Information (Figure S3 and section S4, respectively). The results indicate that the release of the first product, P, is the rate-limiting step (k_3).

All of the fitted rate constants can also be used to calculate the overall value of k_{cat} predicted by this model and its value compared to the experimentally determined steady-state rate. The equation is defined elsewhere (*17*). Using the fitted rate constants from Table 3 with this equation gave a k_{cat} value of 10.7 s^{-1}, which is ~4-fold higher than the experimentally determined parameter. However, this calculation fails to account for the concentration dependence of the second-order rate constant, k_{-3} (the rebinding of P to EQ). An appropriate value for the concentration of P was therefore determined as follows. Given an enzyme concentration of 10 μM and a turnover number of ~3 s^{-1}, about 30 μM product will be formed after 1 s (the duration of the stopped-flow experiments). When the k_{-3} parameter is replaced with $k_{-3}[P]$ ($8.5\ \mu M^{-1}\ s^{-1} \times 30\ \mu M$), the k_{cat} value is 3.7 s^{-1}, which is closer to the experimentally determined value of 2.5 s^{-1}. This question was also addressed more rigorously by simulation, which demonstrated that the model and kinetic parameters account for the observed steady-state rates. This points to the limitations of conventional steady-state analysis in estimating initial velocities based upon the assumption that product inhibition is negligible according to established protocols.

DISCUSSION

Extensive kinetic, mechanistic, and structural studies of microbial dehalogenases have uncovered intriguing catalytic strategies and elucidated many details of these strategies (*22*, *23*). Among the more extensively studied ones are the haloalkane dehalogenases (*23*–*27*), 4-chlorobenzoyl-CoA dehalogenase (*28*–*32*), and CaaD and *cis*-CaaD (*5*, *11*, *21*). These enzymes do not require cofactors and illustrate mechanisms to remove a halogen from alkane, aromatic, and alkene substrates, respectively. In addition to the purely scientific implications of these studies (i.e., how enzymes work), these enzymes may have bioremediation and/or biocatalytic potential (*22*, *23*).

The first two enzymes form a covalent intermediate with the substrate (*22*–*24*, *28*). In the haloalkane dehalogenase from *Xanthobacter autotrophicus* (designated DhlA), the carboxylate group of Asp-124 attacks a carbon of the symmetrical substrate, 1,2-dichloroethane, displaces a chloride, and forms an ester intermediate (*23*, *24*). The departure of the chloride is facilitated by its interaction with two tryptophan residues, Trp-125 and Trp-175, which make up the halide-binding pocket (*25*). Hydrolysis of the ester by water (activated by the catalytic dyad of Asp-260 and His-289) releases the enzyme and the product, 2-chloroethanol. A pre-steady-state kinetic analysis (using 1,2-bromoethane) shows that the chemical steps are slow, but the overall reaction is limited by a conformational change preceding the presumably fast release of the halide (*26*, *27*).

The mechanism of 4-chlorobenzoyl-CoA dehalogenase also involves an ester intermediate but has a different rate-limiting step (*28*–*32*). In this enzyme, Asp-145 attacks the C-4 position (the halide-bearing carbon) of the benzoyl substrate to form the so-called Meisenheimer complex. Rearomatization expels the chloride and generates the arylated Asp-145 (i.e., the ester intermediate) (*28*, *29*). Hydrolysis by a histidine-bound water (His-90) releases HCl and the aspartate group. Pre-steady-state kinetic studies coupled with computational work implicated the formation of the metastable Meisenheimer complex as the rate-limiting step in the overall reaction (*30*–*32*).

[4]Although it was not necessary to invoke a unique fluorescence signal for EQ (from E) to realize a good fit, such a difference could exist. However, by our analysis, EQ does not accumulate, rendering any possible contribution to the overall fluorescence signal negligible and therefore not resolvable.

[5]Standard methods of numerical error analysis assume a Gaussian distribution of error and that the data are independent and identically distributed about the best fit. However, this assumption is not uniformly valid for global fitting because of fluctuations (such as lamp intensity or reactant concentrations) between experiments. Moreover, standard error analysis fails to reveal the complex interrelationships that exist between rate constants and grossly underreports the errors on unconstrained parameters. FitSpace confidence contour analysis probes the relationships between parameters in a pairwise fashion and defines a region of values where both parameters can be varied while still achieving a good fit to the data. A more complete description of this function is found elsewhere (*14*).

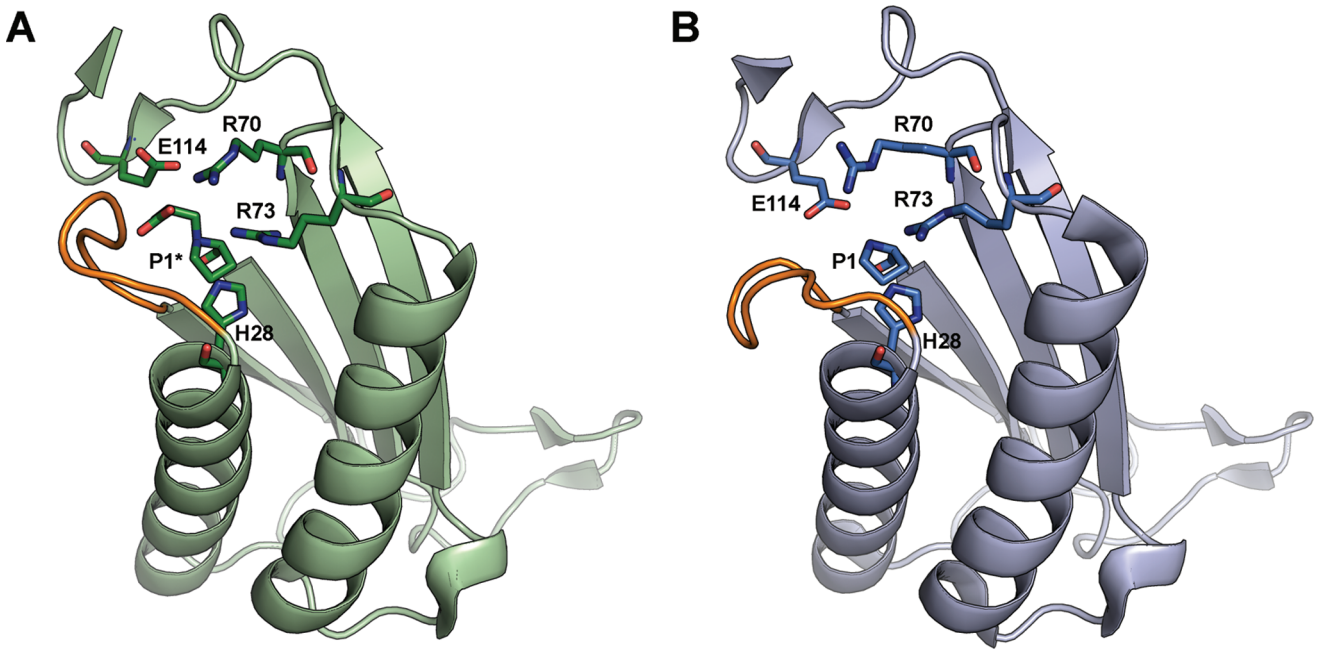

FIGURE 3: The unliganded and covalently modified *cis*-CaaD structures highlighting the loop region, consisting of residues 32−38 (*11*). (A) The active site cavity of *cis*-CaaD after incubation with (*R*)-oxirane-2-carboxylate (green). The figure shows the prolyl nitrogen of Pro-1 attached to (*R*)-2-hydroxypropanoate (P1*). The carboxylate group of the adduct interacts with the backbone amide hydrogen atoms of Phe-37 and Leu-38 of the loop (shown in orange). Glu-114, Arg-70, Arg-73, and His-28 are also shown clockwise. (B) The active site cavity of the unliganded *cis*-CaaD structure (blue). The loop (shown in orange) points away from the active site cavity containing Glu-114, Glu-114, Arg-70, Arg-73, Pro-1, and His-28. This figure was prepared with PyMOL (*33*).

The accumulated sequence, mechanistic, and structural evidence for CaaD and *cis*-CaaD argue against a covalent intermediate (*4*, *5*, *8*−*12*). Instead, the enzymes activate water for attack at the C-3 position of the polarized substrates (Scheme 2). The strategy raises questions about the rate-limiting steps and stability of intermediates. In order to address these questions and place these enzymes into the context of other dehalogenase strategies, we developed methodology for pre-steady-state kinetic analysis. *cis*-CaaD was chosen as the initial system for study because it has a tryptophan (Trp-101) in the active site (*11*), allowing stopped-flow studies. CaaD lacks tryptophan residues such that stopped-flow experiments cannot be readily carried out.

The results provide a description of the kinetic steps in *cis*-CaaD catalysis. In the final kinetic model (Scheme 4), substrate binding is accompanied by an immediate isomerization to a new fluorescent state (i.e., *F*). The new fluorescence signal occurs immediately upon binding of substrate ($E + S \leftrightarrows FS$) within the time resolution of our measurements. One alternative is that there are two steps involving an initial weak binding step followed by a rapid isomerization step ($E + S \leftrightarrows ES \leftrightarrows FS$), but there is insufficient information in the data to accurately resolve the two steps and define a maximum rate of isomerization and ground state K_d. Chemistry occurs next and rapidly in the *FS* complex and produces the *FPQ* complex. If **7** or **8** (Scheme 2) are discrete intermediates, their production and decomposition do not appear to be rate limiting. The final steps involve the release of malonate semialdehyde, which limits the overall reaction and occurs with the return of *F* to its resting fluorescent state *E*, and is followed by the rapid release of bromide.

The identities of *P* and *Q* are tentatively assigned to malonate semialdehyde and bromide, respectively, based on two observations. First, bromide ion competitively inhibits the reaction, indicating that it binds to the free form of the enzyme (i.e., *E*) (*18*−*20*). If, instead, the bromide ion were to bind to the enzyme with one product already bound (*EQ*), then mixed inhibition should have been observed. Second, a second-order rate constant of at least 6 μM^{-1} s^{-1} for the rebinding of product *P* was required for the global fit. This degree of product inhibition is inconsistent with the steady-state bromide inhibition data, which could be satisfactorily fit by simulation with a second-order rate constant of only 5×10^{-4} μM^{-1} s^{-1} (i.e., k_{-4} in Scheme 4). Hence, it is reasonable to propose that malonate semialdehyde is released first (*P*) as the rate-determining step and bromide is released second (*Q*).

One explanation for the difference in fluorescence intensity between the *E* and *F* forms of the enzyme is that they correspond to two conformational states, an open state (i.e., *E*) and a closed state (i.e., *F*). Examination of the native (i.e., unliganded) and inactivated *cis*-CaaD crystal structures raises the possibility that the two states are due to the position of a loop (Figure 3) (*11*). Incubation of *cis*-CaaD with (*R*)-oxirane-2-carboxylate inactivates *cis*-CaaD because the ring-opened species, (*R*)-2-hydroxypropanoate, is covalently attached to the prolyl nitrogen of Pro-1 (*11*, *21*). Comparison of this structure (Figure 3A) with that of the unliganded form (Figure 3B) shows a difference in the positions of the seven-residue loop, comprised of residues 32−38 (Thr-Gly-Thr-Gln-His-Phe-Leu). In the inactivated structure, this loop is closed over the active site cavity where the backbone amide hydrogens of Phe-37 and Leu-38 interact with the carboxylate group of the adduct. The carbonyl of Leu-38 is also within hydrogen-bonding distance of the hydroxy moiety of the adduct rather than the Pro-1 nitrogen (as found in the absence of a covalent inhibitor). In the native form, this same loop points away from the active site. If these observations are reflective of events in the catalyzed reaction, then substrate binding may induce loop closure. If the *F* form is a consequence of substrate binding and active site loop closure, this loop must then reopen (before, during, or after release of the first product), allowing the

enzyme to return to its original form with the second product still bound (*EQ* in Scheme 4).

If loop movement is indeed responsible for the change in fluorescence, then this parameter should be particularly sensitive to mutations in this region. Moreover, it is conceivable that the introduction of "rigidifying" amino acids into this loop could impede the rate of loop closure (i.e., the rate of the *ES* to *FS* transition). It may therefore resolve this step from the preceding binding event ($E + S$), barring any significant effects due to global structure changes. These possibilities are currently being investigated.

ACKNOWLEDGMENT

Electrospray ionization (ESI) mass spectrometry was performed by the Analytical Instrumentation Facility Core (College of Pharmacy, The University of Texas at Austin). We thank Drs. Harold R. Lee, Gerrit J. Poelarends, and William H. Johnson, Jr., for many helpful discussions and suggestions. Stopped-flow and rapid-quench-flow instruments and KinTek Explorer data analysis software were provided by KinTek Corp. (Austin, TX). Financial conflict of interest disclosure: K.A.J. is President of KinTek Corp.

SUPPORTING INFORMATION AVAILABLE

Here we describe the conventional analysis of the pre-steady-state kinetic data (including kinetic schemes and equations used in the fitting process), outline the defining characteristics of the experimental data, evaluate the conventional analysis results, and show why global fitting to a four-step model was required. This is further supported by analysis of the confidence contours and plots for the reversible inhibition of *cis*-CaaD by bromide ion. This material is available free of charge via the Internet at http://pubs.acs.org.

REFERENCES

1. Hartmans, S., Jansen, M. W., van der Werf, M. J., and de Bont, J. A. M. (1991) Bacterial metabolism of 3-chloroacrylic acid. *J. Gen. Microbiol. 137*, 2025–2032.
2. van Hylckama Vlieg, J. E. T., and Janssen, D. B. (1992) Bacterial degradation of 3-chloroacrylic acid and the characterization of *cis*- and *trans*-specific dehalogenases. *Biodegradation 2*, 139–150.
3. Poelarends, G. J., Wilkens, M., Larkin, M. J., van Elsas, J. D., and Janssen, D. B. (1998) Degradation of 1,3-dichloropropene by *Pseudomonas cichorii* 170. *Appl. Environ. Microbiol. 64*, 2931–2936.
4. Poelarends, G. J., Saunier, R., and Janssen, D. B. (2001) *trans*-3-Chloroacrylic acid dehalogenase from *Pseudomonas pavonaceae* 170 shares structural and mechanistic similarities with 4-oxalocrotonate tautomerase. *J. Bacteriol. 183*, 4269–4277.
5. Poelarends, G. J., Serrano, H., Person, M. D., Johnson, W. H., Jr., Murzin, A. G., and Whitman, C. P. (2004) Cloning, expression, and characterization of a *cis*-3-chloroacrylic acid dehalogenase: insights into the mechanistic, structural, and evolutionary relationship between isomer-specific 3-chloroacrylic acid dehalogenases. *Biochemistry 43*, 759–772.
6. Murzin, A. G. (1996) Structural classification of proteins: new superfamilies. *Curr. Opin. Struct. Biol. 6*, 386–394.
7. Poelarends, G. J., Veetil, V. P., and Whitman, C. P. (2008) The chemical versatility of the β-α-β fold: catalytic promiscuity and divergent evolution in the tautomerase superfamily. *Cell. Mol. Life Sci. 65*, 3606–3618.
8. Wang, S. C., Person, M. D., Johnson, W. H., Jr., and Whitman, C. P. (2003) Reactions of *trans*-3-chloroacrylic acid dehalogenase with acetylene substrates: consequences of and evidence for a hydration reaction. *Biochemistry 42*, 8762–8773.
9. de Jong, R. M., Brugman, W., Poelarends, G. J., Whitman, C. P., and Dijkstra, B. W. (2004) The X-ray structure of *trans*-3-chloroacrylic acid dehalogenase reveals a novel hydration mechanism in the tautomerase superfamily. *J. Biol. Chem. 279*, 11546–11552.
10. Azurmendi, H. F., Wang, S. C., Massiah, M. A., Poelarends, G. J., Whitman, C. P., and Mildvan, A. S. (2004) The roles of active-site residues in the catalytic mechanism of *trans*-3-chloroacrylic acid dehalogenase: a kinetic, NMR, and mutational analysis. *Biochemistry 43*, 4082–4091.
11. de Jong, R. M., Bazzacco, P., Poelarends, G. J., Johnson, W. H., Jr., Kim, Y.-J., Burks, E. A., Serrano, H., Whitman, C. P., and Dijkstra, B. W. (2007) Crystal structures of wild type and inactivated *cis*-3-chloroacrylic acid dehalogenase: the structural basis for substrate specificity and inactivation by (*R*)-oxirane-2-carboxylate. *J. Biol. Chem. 282*, 2440–2449.
12. Poelarends, G. J., Serrano, H., Johnson, W. H., Jr., and Whitman, C. P. (2007) The phenylpyruvate tautomerase activity of *trans*-3-chloroacrylic acid dehalogenase: evidence for an enol intermediate in the dehalogenase reaction? *Biochemistry 46*, 9596–9604.
13. Johnson, K. A., Simpson, Z. B., and Blom, T. (2009) Global kinetic explorer: a new computer program for dynamic simulation and fitting of kinetic data. *Anal. Biochem. 387*, 20–29.
14. Johnson, K. A., Simpson, Z. B., and Blom, T. (2009) FitSpace explorer: an algorithm to evaluate multidimensional parameter space in fitting kinetic data. *Anal. Biochem. 387*, 30–41.
15. Waddell, W. J. (1956) A simple ultraviolet spectrophotometric method for the determination of protein. *J. Lab. Clin. Med. 48*, 311–314.
16. Laemmli, U. K. (1970) Cleavage of structural proteins during the assembly of the head of bacteriophage T4. *Nature 227*, 680–685.
17. Johnson, K. A. (1992) Transient-state kinetic analysis of enzyme reaction pathways, in The Enzymes (Sigman, D. S., Ed.) 3rd ed., pp 1−61, Academic Press, San Diego.
18. Cornish-Bowden, A. (1974) A simple graphical method for determining the inhibition constants of mixed, uncompetitive and non-competitive inhibitors. *Biochem. J. 137*, 143–144.
19. Dixon, M. (1953) The determination of enzyme inhibitor constants. *Biochem. J. 55*, 170–171.
20. Cornish-Bowden, A. (2004) Fundamentals of Enzyme Kinetics , 3rd ed., pp 121−123, Portland Press, London.
21. Poelarends, G. J., Serrano, H., Johnson, W. H., Jr., and Whitman, C. P. (2004) Stereospecific alkylation of *cis*-3-chloroacrylic acid dehalogenase by (*R*)-oxirane-2-carboxylate: analysis and mechanistic implications. *Biochemistry 43*, 7187–7196.
22. Copley, S. D. (1999) Microbial dehalogenases, in Comprehensive Natural Products Chemistry (Barton, D., and Nakanishi, K., Eds.) Vol. 5, pp 401−422, Elsevier, Amsterdam.
23. Janssen, D. B. (2004) Evolving haloalkane dehalogenases. *Curr. Opin. Chem. Biol. 8*, 150–159.
24. Verschueren, K. H., Seljée, F., Rozeboom, H. J., Kalk, K. H., and Dijkstra, B. W. (1993) Crystallographic analysis of the catalytic mechanism of haloalkane dehalogenase. *Nature 363*, 693–698.
25. Verschueren, K. H., Kingma, J., Rozeboom, H. J., Kalk, K. H., Janssen, D. B., and Dijkstra, B. W. (1993) Crystallographic and fluorescence studies of the interaction of haloalkane dehalogenase with halide ions. Studies with halide compounds reveal a halide binding site in the active site. *Biochemistry 32*, 9031–9037.
26. Schanstra, J. P., Kingma, J., and Janssen, D. B. (1996) Specificity and kinetics of haloalkane dehalogenase. *J. Biol. Chem. 271*, 14747–14753.
27. Schanstra, J. P., and Janssen, D. B. (1996) Kinetics of halide release of haloalkane dehalogenase: evidence for a slow conformational change. *Biochemistry 35*, 5624–5632.
28. Benning, M. M., Taylor, K. L., Liu, R.-Q., Yang, G., Xiang, H., Wesenberg, G., Dunaway-Mariano, D., and Holden, H. M. (1996) Structure of 4-chlorobenzoyl coenzyme A dehalogenase determined to 1.8 Å resolution: an enzyme catalyst generated via adaptive mutation. *Biochemistry 35*, 8103–8109.
29. Zhang, W., Wei, Y., Luo, L., Taylor, K. L., Yang, G., Dunaway-Mariano, D., Benning, M. M., and Holden, H. M. (2001) Histidine 90 function in 4-chlorobenzoyl-coenzyme A dehalogenase catalysis. *Biochemistry 40*, 13474–13482.
30. Liu, R.-Q., Liang, P.-H., Scholten, J., and Dunaway-Mariano, D. (1995) Transient state kinetic analysis of the chemical intermediates formed in the enzymatic dehalogenation of 4-chlorobenzoyl-coenzyme A. *J. Am. Chem. Soc. 117*, 5003–5004.
31. Xu, D., Wei, Y., Wu, J., Dunaway-Mariano, D., Guo, H., Cui, Q., and Gao, J. (2004) QM/MM studies of the enzyme-catalyzed dechlorination of 4-chlorobenzoyl-CoA provide insight into reaction energetics. *J. Am. Chem. Soc. 126*, 13649–13658.
32. Wu, J., Xu, D., Lu, X., Wang, C., Guo, H., and Dunaway-Mariano, D. (2006) Contributions of long-range electrostatic interactions to 4-chlorobenzoyl-CoA dehalogenase catalysis: a combined theoretical and experimental study. *Biochemistry 45*, 102–112.
33. DeLano, W. L. (2002) The PyMOL molecular graphics system, DeLano Scientific, San Carlos, CA (http://www.pymol.org).